

Superior, processing-dependent thermal conductivity of cellulose Nanocrystal-Poly(vinyl alcohol) composite films

Reaz A. Chowdhury^{a,1}, Amit Rai^{b,1}, Evan Glynn^b, Patrick Morgan^b, Arden L. Moore^{b,**}, Jeffrey P. Youngblood^{a,*}

^a School of Materials Engineering, Purdue University, 701 W. Stadium Ave., West Lafayette, IN, 47907, USA

^b Institute for Micromanufacturing, Louisiana Tech University, 911 Hergot Ave., Ruston, LA, 71272, USA



HIGHLIGHTS

- CNC-PVA composite films were prepared with a variation of order parameter between 0 and 0.85 for anisotropic films.
- PVA molecules act as an interstitial filler between the CNCs, hence improving the effective κ of the CNC-PVA composite films.
- Anisotropic CNC-PVA films showed κ as high as $\sim 3.45 \text{ W m}^{-1} \text{ K}^{-1}$, the highest value reported for a CNC-based material to-date.
- Our CNC-PVA composite films exhibited $\sim 4\text{--}14$ fold higher κ than that of films for flexible electronic devices.

ARTICLE INFO

Keywords:

Thermal conductivity
Cellulose nanocrystals
Organic composites
Hermans order parameter
Flexible electronics

ABSTRACT

The in-plane thermal conductivity of cellulose nanocrystal (CNC) – poly(vinyl alcohol) (PVA) composite films containing different PVA molecular weights, CNC loadings and varying order parameters (S) were investigated as an eco-friendly, renewable and sustainable alternative to commonly used petroleum-based polymeric materials for potential application in thermal management of flexible electronics. Isotropic CNC-PVA bulk films with 10–50 wt% PVA solid loading showed significant improvement in thermal conductivity compared to either one component system. Further, anisotropic composite films exhibited in-plane thermal conductivity as high as $\sim 3.45 \text{ W m}^{-1} \text{ K}^{-1}$ in the chain direction, which is higher than most polymeric materials used as substrates for flexible electronics. Such an improvement can be attributed to the inclusion of PVA as well as to a high degree of CNC orientation. Further, a theoretical model was used to study the effect of CNC arrangement (both isotropic and anisotropic configuration) and interfacial thermal resistance on the in-plane thermal conductivity of the CNC-PVA composite films. In order to demonstrate an application for flexible electronics, thermal images of a concentrated heat source on both neat PVA and CNC-PVA composite films were taken that showed the temperature of the resulting hot spot was lower for the composite films at the same power dissipation.

1. Introduction

Thermal management has become a critical issue for electronic devices due to escalating power densities and an increasing reliance on polymeric packaging materials. In traditional rigid electronics, electrically insulating polymers are extensively used as printed circuit boards (PCBs), device holders, or thermal interface materials (TIMs) due to the ease of processability, low cost, and low density compared to other materials [1,2]. Typical thermal conductivity (κ) values for neat, amorphous polymers are very low (typically $0.1\text{--}0.3 \text{ W m}^{-1} \text{ K}^{-1}$

[1–3]), which causes a major bottleneck in terms of thermal management. Recently, there has been growing interest towards flexible electronics because of their potential applications in sensors, displays, energy harvesting, and electronic skins for robotics [4]. Flexible electronics also face issues of thermal management as the entire supporting substrate is usually comprised of a low κ material. Plastic-based materials such as polyethylene terephthalate (PET), polyethylene naphthalate (PEN), and polyimide (PI) are popular for such applications since they are mechanically strong, chemically stable, optically transparent, easy to fabricate, and have industrial-scale production

* Corresponding author.

** Corresponding author.

E-mail addresses: amooore@latech.edu (A.L. Moore), jpyoungb@purdue.edu (J.P. Youngblood).

¹ These authors contributed equally.

capability through roll-to-roll printing methods [5]. However, these petroleum-based materials are environmentally less attractive from a life-cycle point-of-view [6] and have low κ of $\sim 0.15\text{--}0.3\text{ W m}^{-1}\text{ K}^{-1}$ at ambient conditions similar to those used in traditional electronics packaging [7–9]. For materials with low κ , even modest power densities can lead to overheating and, ultimately, permanent damage to the device [10]. Overheating in electronics in general has been cited as a major factor in $\sim 55\%$ of electronic equipment failures which are attributed to malfunction, PCB board failure, or short circuit [11,12].

To improve the κ of polymers used in electronics packaging, several types of inorganic fillers such as boron nitride (BN), metal nitride, metallic nanowires, carbon materials, metal oxide or clay have been used in the polymer matrix [1,13–17]. However, the addition of such fillers may sacrifice other important polymer properties such as processability or electrical insulation. For example, carbon nanotubes (CNTs) have extremely high κ , but their application in polymer nanocomposites is limited due to the presence of high interfacial resistance (between nanotube and matrix) and high contact resistance (between nanotubes) [14]. Graphene or graphite nanoplatelets in a polymer matrix can overcome the interfacial resistance issue and exhibit superior κ but at the expense of sacrificing electrical insulation [18–20]. In terms of processability, while including a greater percentage of particulates can increase a composite's κ , it also has a strong effect on viscosity which may make integration into electronics packaging impossible [21]. Due to the above circumstances, researchers continue to search for new substrate materials that are environmentally friendly, highly flexible, and at the same time thermally conductive in order to alleviate local heating from flexible electronic devices.

Cellulose-based materials are considered to be potential candidates as eco-friendly substrates of flexible electronic devices with the capability of resolving thermal management issues [22]. Cellulose derivatives are attractive bio-materials regarding environmental (low toxic, low carbon footprint, and biodegradable) and economical (abundant, renewable, and easily recyclable) concerns [23]. In addition, the low coefficient of thermal expansion and high mechanical strength of such materials show their potential for next-generation flexible electronic device substrates. However, few studies have been reported regarding the thermal properties of cellulose-based materials for their applications as substrates for flexible electronic devices. Shimazaki et al. created a highly thermally conductive cellulose nanofiber/epoxy resin nanocomposite with a κ of $\sim 1.1\text{ W m}^{-1}\text{ K}^{-1}$, which was nearly seven times higher than that of the neat epoxy matrix ($0.15\text{ W m}^{-1}\text{ K}^{-1}$) [24]. Such a high value of κ was attributed to the crystalline nature of cellulose nanofibers that provide excellent phonon pathways through the nanocomposite. Uetani et al. observed in-plane κ values as high as $\sim 2.5\text{ W m}^{-1}\text{ K}^{-1}$ for tunicate nanowhiskers (TNWs), which was about eight times higher than in the thickness direction due to the fiber orientation in heat flow direction [22]. In another study, Uetani et al. reported the in-plane κ value as high as $\sim 2.5\text{ W m}^{-1}\text{ K}^{-1}$ for nanocellulose (NC)-acrylic resin composite, which was more than three times higher than the κ of the neat acrylic resin ($\sim 0.76\text{ W m}^{-1}\text{ K}^{-1}$) [25]. This value is roughly an order of magnitude higher than those of the plastic films that are currently used for flexible electronics substrates, and hence shows the potential of cellulose-based materials for use as the substrate to efficiently cool the next generation flexible electronic devices.

Of the various forms of cellulose, cellulose nanocrystals (CNCs) are intriguing from an engineering materials perspective. CNCs are rod-like anisotropic nanoparticles that possess a unique set of properties such as low density, high specific strength, optical transparency, and electrical insulation [23]. The material properties (mechanical, thermal, electrical, and optical) of CNC-based materials can be controlled with the structural arrangement of the crystalline domains [26–28]. However, the organization of crystalline anisotropic domains within a CNC-based material is strongly influenced by the processing history, with the final arrangement being isotropic, chiral nematic, or anisotropic [29].

Experimentally, chiral nematic and anisotropic transverse directions show four-fold lower κ compared to in the anisotropic longitudinal (aligned) direction [30]. Based on this current understanding of the processing-structure-property relationship within CNC-based films, increased packing density with strong interfacial interaction are expected to be effective routes to enhancing the κ of CNC-based materials, which may act as an alternative for flexible electronic substrates to resolve the issue of thermal management.

Previous work(s) have examined the structure-property relationship for CNC-only films, with interstitial spaces between CNCs representing void space. Filling the void space with a compatible polymer with lower interfacial resistance should increase the κ by providing additional paths for phonon propagation between crystallites. In this context, PVA can be an excellent candidate to be a binding agent as it is a waterborne polymer with an abundance of hydroxyl moieties that can form relatively strong hydrogen bonds to form a stable network structure among CNCs. In this work, we created CNC-PVA composite films of varying internal structure and examine how processing affects the CNC ordering and, thus, the films' κ magnitude and directional dependence. Isotropic and anisotropic structural arrangements of CNCs in the composite films were prepared for various CNC:PVA ratios that governed the phonon scattering by controlling the available free volume in the composite films. The in-plane κ of the CNC-PVA composite films were determined using a modified steady-state bridge method. A combination of experimentation and modeling was used to study the effects of addition of PVA on the effective κ of the CNC-based films and the interfacial thermal resistance.

2. Experimental methods

2.1. CNC film preparation and CNC alignment characterization

Never-dried, pristine CNC aqueous suspension (12.2 wt%, batch no-2015-FPL-071CNC) with 1% sulfur and sodium counterion was purchased from the University of Maine (Orono, ME, USA) and manufactured by the USDA, US Forest Service-Forest Products Laboratory. Poly(vinyl alcohol) (PVA) with different molecular weights were purchased from Sigma-Aldrich. Different properties such as molecular weight, crystallinity index and hydrolysis information for PVA can be found in the supporting information section. All materials were used as received without any modification.

2.1.1. Film fabrication

CNC-PVA composites with random/chiral nematic configuration were prepared from compositions as shown in Table S1. Briefly, a 20 ml solution was poured in a polystyrene Petri dish and slow evaporation (several days) at room temperature was utilized for the film fabrication. Two different approaches were used for oriented film fabrication. Anisotropic CNC films were prepared with a method reported by Reising et al. where about 300 S^{-1} shear rate was applied for shear alignment [26]. Samples were dried at room temperature for several days. Finally, anisotropic CNC-PVA composites was prepared by Roll-to-Roll microgravure coating where details of the procedure can be found in the literature [31]. Here, PET was used as a flexible substrate and the overall fabrication was performed at a 32 rpm microgravure rotation with 0.63 m/min substrate speed. The drying oven temperature was 85°C and the completely dried coated film was received in the re-winder.

2.1.2. Orientation measurement

A conventional UV-Vis spectrophotometer (spectra max Plus 384, molecular devices Corp., Sunnyvale, CA) was used for the order parameter measurement. A similar method described by Chowdhury et al. was used for this characterization, with additional details in Ref. [28]. Briefly, a 12mmX25 mm free standing sample was placed between a cross polarizer and the transmittance data was measured for 45° and

90° configuration. The transmitted signal was measured from 400 to 750 nm wavelength. The following equations were utilized for the order parameter (S) calculation:

$$I = I_0 \sin^2 2\theta \sin^2 \left(\frac{\pi \Delta n d}{\lambda} \right) \quad (1)$$

So

$$\frac{I_{45}}{I_{90}} = \frac{I_0 \sin^2(2 * 45) \sin^2 \left(\frac{\pi \Delta n d}{\lambda} \right)}{I_0 \sin^2(2 * 90) \sin^2 \left(\frac{\pi \Delta n d}{\lambda} \right)}$$

Hence

$$\frac{I_{45}}{I_{90}} = D * = D. g = \frac{(2S + 1)}{(1 - S)} \quad (2)$$

Here, I_0 , θ , Δn , d , λ , I , g and D represents amplitude of incident light, sample position with respect of polarizer, refractive index difference, sample thickness, wavelength of incident light, transmitted light intensity, correction factor and dichroic ratio, respectively. As the refractive index difference for ordinary light and extraordinary light is insignificant, $g = 1$ was used for the calculation. Finally, the order parameter for any material is between 0 and 1 where, $S = 0$ defined as random/isotropic configuration and $S = 1$ is for perfect anisotropic configuration.

2.2. Phase morphology of the composite films

A Carl Zeiss (Axio observer A1) inverted polarized light microscopy in transmission mode was used for the characterization of phase morphology for CNC and PVA components. Briefly, samples were oriented in 45° and 90° positions with respect to the plane of polarized light. It should be noted that the samples at 45° and 90° position formed bright field and dark field illumination, respectively. The fracture surface of the composite films was observed by a scanning electron microscopy (SEM, ProX, Phenom). Before imaging, a thin layer of gold coating was sputtered on the samples.

2.3. Thermal conductivity measurement

The in-plane κ of the CNC films near room temperature were measured using a modified steady-state bridge method similar to the one employed by Benford et al. to measure κ of free-standing tape/thin films [32]. An annotated 3D illustration of the measurement stage used in this work is given in Fig. 1. The measurement stage consists of two

identical platforms, each of which is comprised of a 25 mm x 7 mm x 1 mm copper (Cu) plate, backside serpentine Nichrome wire heater, PFA-insulated 0.127 mm diameter Type J thermocouple, and a 20 mm long 2 mm diameter threaded Nylon support. Each Nylon platform support is anchored to an adjustable stainless-steel base with thermal mass much larger than that of the platforms. During measurements, electrical power is supplied to one of the platforms via 15 cm long, 0.255 mm diameter insulated lead wires (2 per platform) that attach to the Nichrome heater at the copper plate. This localizes Joule heating to the Nichrome wire heater that is in direct contact with the copper plate, while also minimizing parasitic heat conduction along the leads. It should be noted that both platforms are identical for the sake of the thermal circuit analysis used to determine κ , but that only one Nichrome heater is powered during a given experiment.

For sample preparation and mounting, rectangular sections 3–5 mm in width and up to 25 mm in length were first cut from the CNC film under study. For anisotropic films, this was done either perpendicular or parallel to the direction of crystal alignment. When possible, multiple sections of sample were stacked together to increase signal strength relative to background. Samples were affixed on either end to the Cu plates using a vacuum-compatible high conductivity silver paint (SPI Supplies). This left a segment of clean film sample with known length, width, and total thickness suspended between the two copper plates as shown in Fig. 1. The entire stage assembly was then loaded into a vacuum chamber and pumped down to $\sim 10^{-6}$ Torr via mechanically-backed turbo pump to minimize convection heat transfer. Electrical power and thermocouple leads extended across the chamber walls via a vacuum-compatible feedthrough.

Once the vacuum was stabilized, κ measurements could begin by inducing Joule heating in one of the Nichrome heaters via a precision DC power supply. This raised the temperature of the corresponding Cu platform, with heat being conducted along the suspended length of the sample as through the support and leads. The setup allows for measurement of the Joule heating in the Nichrome heater as well as the temperature of each Cu platform, from which the κ of the film sample can be determined via conduction analysis of the setup's thermal circuit as described in our previous work [30]. To reduce measurement uncertainty, steady-state temperature differences were measured at multiple Joule heating powers for each sample and the observed linear trend of temperature difference versus heat conducted through the sample used to determine the sample's thermal resistance. Heat conduction through residual air within the chamber was accounted for by performing the measurement without a sample present to obtain the "background" thermal conductance and subtracting this from the thermal conductance values obtained with a sample present. The total measured thermal conductance was found to be at least 2X this background thermal conductance for all samples. The major source of experimental uncertainty stems from the inherent accuracy of two thermocouples (± 1.1 °C). When this inherent accuracy for a single thermocouple is propagated forward to measuring a temperature difference with two identical thermocouples, the uncertainty in the temperature difference becomes ± 1.6 °C. For context, during a typical measurement the maximum temperature difference between the heating and sensing platforms was generally ~ 10 – 13 °C. The use of the linear slope method described above involving multiple data points helps reduce the magnitude of this error, although it still dominates those associated with sample geometry, applied Joule heating, and parasitic heat losses. When considering all of these sources of error and using standard error propagation for both measurements (background and with sample present), an upper limit of $\pm 19.2\%$ measurement uncertainty in thermal conductivity is associated with the results presented in this work. For future work, the overall measurement uncertainty could be significantly improved through the use of alternative temperature measurement methods which offer superior accuracy, such as well-calibrated silicon diodes.

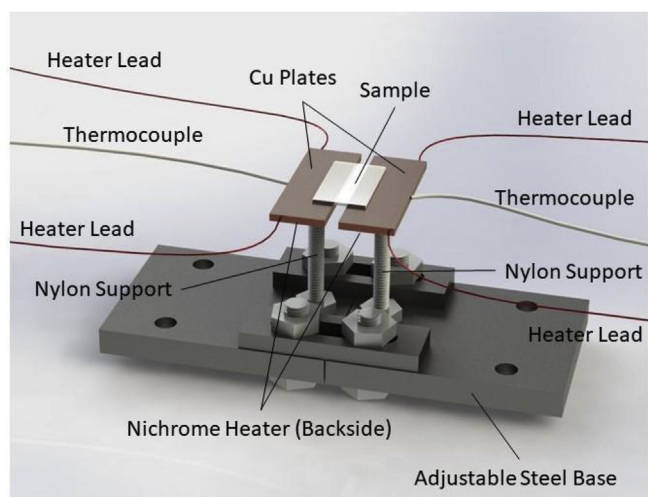


Fig. 1. Annotated 3D drawing of the measurement stage. Silver paint for affixing the sample not shown.

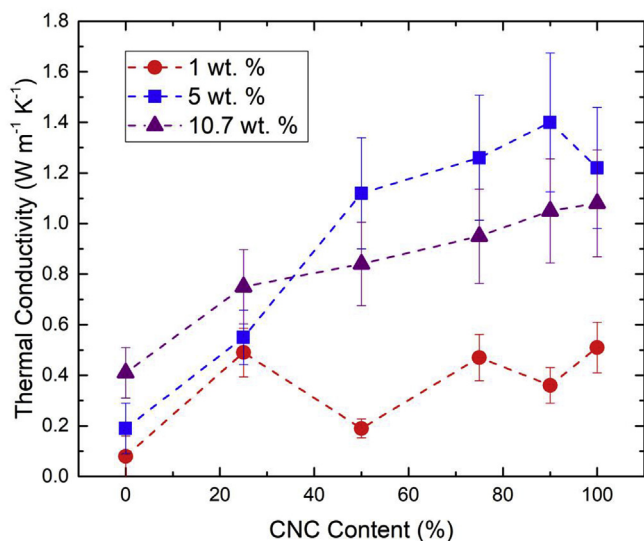


Fig. 2. Thermal conductivity of un-sheared CNC:PVA films versus CNC content of final film. Data shown is for 1, 5, and 10.7 initial CNC and PVA weight percent used during fabrication. The PVA molecular weight was 124–186 K.

3. Results and discussion

3.1. Effect of (CNC: PVA) composition with isotropic configuration

The κ of any polymer nanocomposite system depends on aspects of its internal structure such as nanofiller percentage, aspect ratio of nanofiller, nanofiller orientation, and the matrix-filler interaction, which collectively also determine the free volume (as an active defect site) of polymer segments; in short, how the structure affects phonon propagation and scattering within the material [1]. Figs. 2 and 3 present the measured κ of CNC-PVA composite films with differing CNC to PVA ratios made with 124–186 K and 89–98 K PVA molecular weight, respectively. As structure of the nanocomposite can be affected by fluidity of the solution during drying, the effect of dilution factor on κ was investigated for three different initial concentrations (from dilute to concentrated solution). For both figures, increasing CNC percentage generally leads to higher κ compared to neat PVA (0% CNC) results. The long-chain PVA showed very low κ , likely due to the presence of

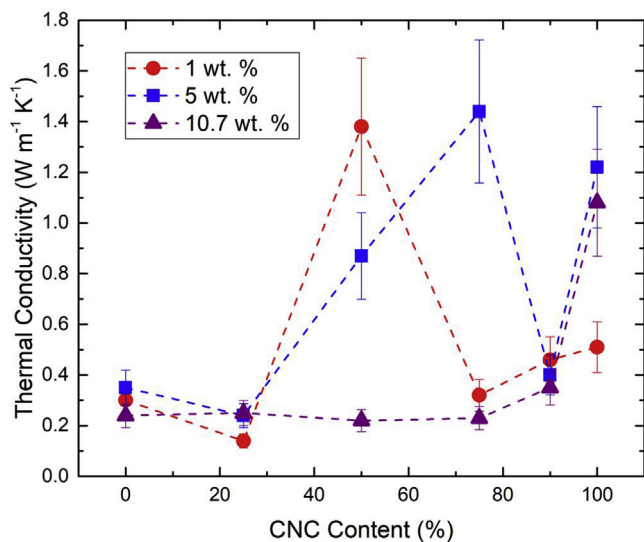


Fig. 3. Thermal conductivity of un-sheared CNC:PVA films versus CNC content of final film. Data shown is for 1, 5, and 10.7 initial CNC and PVA weight percent used during fabrication. The PVA molecular weight was 89–98 K.

entanglements with a globular structure, which provide additional free volume; hence, higher phonon scattering. Bulk PVA films with different concentrations and molecular weights showed κ between 0.1 and $0.4 W m^{-1} K^{-1}$. Higher concentration and molecular weight PVA leads to a higher viscosity of the solution, which may affect the morphology of the resultant composites. Alternatively, lower concentrations would lead to more void space left from solvent evaporation, which would decrease conductivity. During drying, higher molecular weights, with the concomitant higher viscosity may affect relaxation dynamics leading to different packing densities. PVA films with higher packing density should have higher κ compared to lower packing density, which are the major reason for the variable thermal conductivity. However, the values obtained are within the range expected for such polymers. Bulk CNC films (100% CNC) with different initial concentration showed variable κ , with the best results obtained for initial concentrations above 1%. It is well known that, never-dried CNC suspensions can possess chiral nematic configuration which is strongly concentration dependent [33,34]. Higher concentration CNC suspensions may not have well organized chiral nematic structure due to frustrated ordering, so can instead be highly defected and nearly random while dilute CNC suspensions may have an organized chiral nematic configuration. However, a chiral nematic structure may have more free volume in the system that will be responsible for phonon scattering and therefore a low κ as was observed in this work. Moreover, CNCs are in a random configuration in the transverse and longitudinal direction due to the generally isotropic (or orthotropic) arrangement. The phase morphology for isotropic CNC-PVA films can be found in the supporting information section. Thus, the results given in Figs. 2 and 3 represent values associated with a generally isotropic CNC orientation within the in-plane direction.

With the addition of PVA in the CNC suspension with different concentrations, the resulting films can have random or chiral nematic structure, which is determined by the initial concentration of nanocomposite aqueous suspension, PVA molecular weight and PVA solid loading (Table S1 in the supporting information section). The κ for CNC-PVA composites were very different than expected. Pure CNC film showed significantly higher κ (at least 2–6 fold) compared to neat PVA films and was concentration dependent. However, this binary composite system did not follow a general rule of mixtures. It was observed that PVA (Mw: 124–186 K) solid loading between 10 and 25 wt% showed an improved κ for CNC-PVA composites. Results for the lower molecular weight PVA (Mw: 89–98 K) are more complex, showing an increase in the κ with PVA solid loading between 25 and 50 wt% that also depended on the initial solution concentration.

Based on the experimental evidence, it can be deduced that a maximum κ can be observed at the higher CNC solid loading region where PVA molecules can act as a binder or interstitial filler between the CNCs. The addition of PVA must therefore reduce the effective interfacial thermal resistance for this binary composite system compared to the pristine CNC materials (Fig. 4). The effect of PVA for the reduction of interfacial resistance has been discussed in the supporting information section. PVA molecules contain hydroxyl groups which can form hydrogen bonds with the CNCs, which are relatively strong and therefore have low interfacial resistance. Further, by filling the voids between CNCs, which would otherwise be air, the PVA helps form a continuous thermal network [35]. As in percolation theory, PVA solid loading should be in an optimum percentage to form a homogeneous network structure for this improved κ [35]. However, the data suggests that PVA loading is dependent on the CNC organization and the molecular weight of the PVA.

3.2. Effect of anisotropy for different CNC: PVA composition

Due to the anisotropy of the crystalline directions of individual CNCs, they transmit thermal energy differently in each (longitudinal and transverse) direction relative to its primary axis. Therefore, the κ

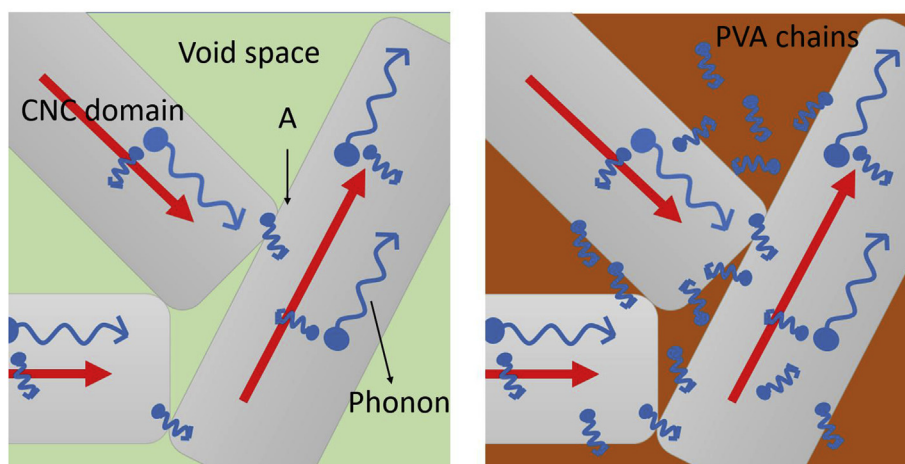


Fig. 4. Effect of PVA for reducing the interfacial resistance between CNC domains. Here, point A is showed for interfacial contact position where phonon can diffuse from one crystal to another crystal. (red arrow sign is denoted for the sum of every phonon vector projection in the chain direction of individual crystalline domain). (For interpretation of the references to colour in this figure legend, the reader is referred to the Web version of this article.)

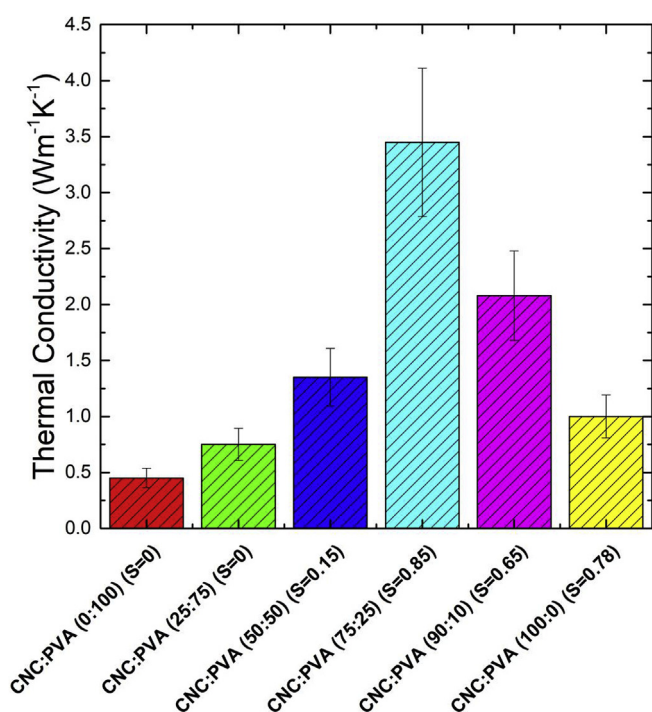


Fig. 5. In-plane thermal conductivity in the direction of shear of CNC-PVA nanocomposites with various degrees of orientation. S is Hermans order parameter for CNC-PVA nanocomposite system.

for bulk CNC film should depend on the CNC crystalline organization and likewise be anisotropic in films with anisotropic organization/orientation. As predicted, an anisotropic arrangement is shown to have a significant increase in the κ for CNC-PVA nanocomposite system (Fig. 5). An analysis of variance (ANOVA) study using Tukey's approach of multiple pairwise comparisons was conducted at 95% confidence level for the data plotted in Fig. 5. The outcome of this comparison was that statistically significant differences existed between CNC:PVA (75:25) results and those of all other sample types. A statistically significant difference was also determined to exist between results for CNC:PVA (90:10) and the two lowest CNC content sample types, specifically CNC:PVA (0:100) and CNC:PVA (25:75). All other inter-sample statistical comparisons did not reveal statistically significant differences.

Solution casting methods based on roll-to-roll processing were used for this fabrication, and no significant alignment (i.e. order parameter $S \sim 0$) was observed for PVA solid loading higher than 50 wt%. PVA

long chain molecules in aqueous suspension have a globular structure with many entanglements. The applied shear is insufficient to align it in the shear direction⁴⁵. When PVA loading is less than 25 wt%, however, it is possible for it to be entrapped between CNC domains. In this case, the film anisotropy is dominated by CNC liquid crystallinity. Hence, anisotropy was observed for CNC-PVA composite coatings with CNC loading higher than 50 wt%. The phase morphology for a typical anisotropic CNC-PVA composite film can be found in the supporting information section.

CNC-PVA composite films with anisotropic configurations demonstrated higher κ compared to the corresponding isotropic configuration, but only along the directions of alignment and was highly dependent on the degree of ordering, i.e. the order parameter S . Experimentally, films with an anisotropic arrangement of CNC-PVA (75:25) composition showed 2.5 times improvement in thermal conductivity along the shear direction compared to films with an isotropic configuration with the same composition. Maximum orientation was observed for this composition ratio, which is the prime reason for the exceptionally high observed κ . Unlike Fig. 4, individual CNCs are aligned uniaxially (along the shear direction) which allows phonon propagation down the highest κ direction of the CNC (Fig. 6). Moreover, aligning the CNCs allows more interfacial contact between the CNCs for higher phonon transport across the interface (details can be found in the supporting information section). As in the isotropic case, the interfacial resistance between two CNCs is reduced by the PVA filling of the void space and the high bond strength of the PVA molecules. As mentioned before, the PVA percentage should have an optimum percentage with CNC (based on percolation theory) that can act as binder for CNC domains [35]. Other CNC-PVA compositions showed moderate to very low anisotropy, hence, the improvement of κ along the shear direction would not be expected to as high.

It is also worth mentioning that κ reported here is much higher than the traditionally used electrically insulating polymers and associated nanocomposite systems. A comparative data with different polymer systems has been shown in Table 1.

3.3. Effective medium theory – Choy & Young (EMT-CY) model applied to CNC-PVA composite thin films

For any polymer nanocomposite, the interfacial thermal resistance (ITR) between the fillers and between the filler and matrix plays a significant role in the overall thermal transport. For structured materials, anisotropy also plays a central role, as is the case here. Different models are available to describe complex nanostructured materials [37], polycrystalline structures [38], and composites [39] where the interfaces and the organization of the materials are factors that dominate the thermal properties. Choy and Young [40] developed a model

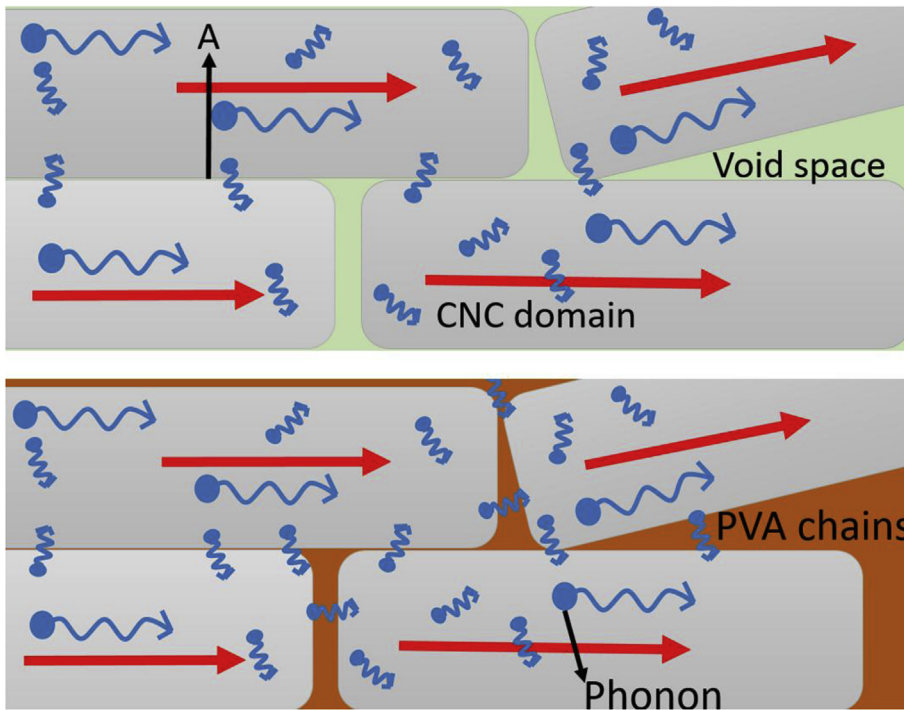


Fig. 6. Effect of PVA for reducing the interfacial resistance between CNCs for anisotropic composites. Here, point A is shown for the interfacial contact position where phonons can diffuse from one crystal to another crystal. (red arrow sign is denoted for the sum of every phonon vector projection in the chain direction of individual crystalline domain). (For interpretation of the references to colour in this figure legend, the reader is referred to the Web version of this article.)

with an adaptation of Maxwell's effective medium theory [41] (denoted EMT-CY here), which has been previously applied to study the change in the κ of oriented semi-crystalline polymers [42–44] both along and normal to the orientation direction as a function of the orientation direction crystallinity.

The expressions derived from the EMT-CY model for the CNC-PVA nanocomposites are [40]

$$\frac{\kappa_c - \kappa_m}{\kappa_c + 2\kappa_m} = x \left[\frac{2}{3} \left(\frac{\lambda_{\perp} - 1}{\lambda_{\perp} + 2} \right) + \frac{1}{3} \left(\frac{\lambda_{\parallel} - 1}{\lambda_{\parallel} + 2} \right) \right] \quad (3)$$

$$\frac{\kappa_{\perp} - \kappa_m}{\kappa_{\perp} + 2\kappa_m} = x \left[\left(\frac{\lambda_{\perp} - 1}{\lambda_{\perp} + 2} \right) \left(\frac{1 + \langle \cos^2 \gamma \rangle}{2} \right) + \left(\frac{\lambda_{\parallel} - 1}{\lambda_{\parallel} + 2} \right) \left(\frac{\langle \sin^2 \gamma \rangle}{2} \right) \right] \quad (4)$$

$$\frac{\kappa_{\parallel} - \kappa_m}{\kappa_{\parallel} + 2\kappa_m} = x \left[\left(\frac{\lambda_{\perp} - 1}{\lambda_{\perp} + 2} \right) \langle \sin^2 \gamma \rangle + \left(\frac{\lambda_{\parallel} - 1}{\lambda_{\parallel} + 2} \right) \langle \cos^2 \gamma \rangle \right] \quad (5)$$

$$\lambda_{\perp} = \frac{\kappa_{c\perp}}{\kappa_m} \quad (6)$$

$$\lambda_{\parallel} = \frac{\kappa_{c\parallel}}{\kappa_m} \quad (7)$$

$$S = \frac{3 \langle \cos^2 \gamma \rangle - 1}{2} \quad (8)$$

where x is the weight fraction of the CNC, which is approximately 0.75 for the samples under study [30] (details about selection of the value of x can be found in the supporting information section), and κ_c is the thermal conductivity of an isotropic film which is approximated as $1.22 \text{ W m}^{-1} \text{ K}^{-1}$ from our measurement results presented previously in this work. The effective matrix thermal conductivity κ_m is obtained by solving Equations (3), (6) and (7) simultaneously. Equations (4) and (5) are used to calculate the macroscopic κ of the CNC-PVA composite films in the directions parallel (κ_{\parallel}) and perpendicular (κ_{\perp}) to the shear

Table 1
Thermal conductivity for different polymer/polymer nanocomposite systems.

Sample	Matrix (wt%)	Filler (wt%)	S	κ	References
PPS-BN	PPS-(70)	BN-(30)	–	0.62	[15]
Epoxy-graphite	Epoxy- (76)	Graphite- (24)	–	1.8	[36]
Epoxy-CNF	Epoxy	CNF	–	0.35	[36]
HDPE-Al	HDPE- (80)	Al- (20)	–	0.7–1.25	[1]
Common Engineering thermoplastic	Polymer as matrix	No filler	–	0.11–0.53	[1]
PMMA-CNT	PMMA- (96)	CNT- (4)	–	3.4	[14]
Acrylic resin-NC	Acrylic resin	NC	–	2.5	[25]
TNW	TNW	–	–	2.5	[13]
PI	PI	–	–	0.91	[13]
PET	PET	–	–	0.87	[13]
COP	COP	–	–	0.70	[13]
PPS	PPS	–	–	0.63	[13]
PA	PA	–	–	0.25	[13]
PES	PES	–	–	0.25	[13]
CNC-PVA	CNC	PVA	0	1.4 (maximum)	This work
CNC-PVA	PVA	CNC	0	0.7 (maximum)	This work
CNC-PVA	CNC	PVA	0.85–0.65	3.5 (maximum)	This work

PPS = Polyphenylene sulfide; CNF = Cellulose nanofiber; HDPE = High-density polyethylene; PMMA = Poly(methyl methacrylate); TNW = Tunicate nanowhisker; NC = Nanocellulose; COP = Cyclo-olefin polymer; PA = Polyamide; PES = Polyethesulfone.

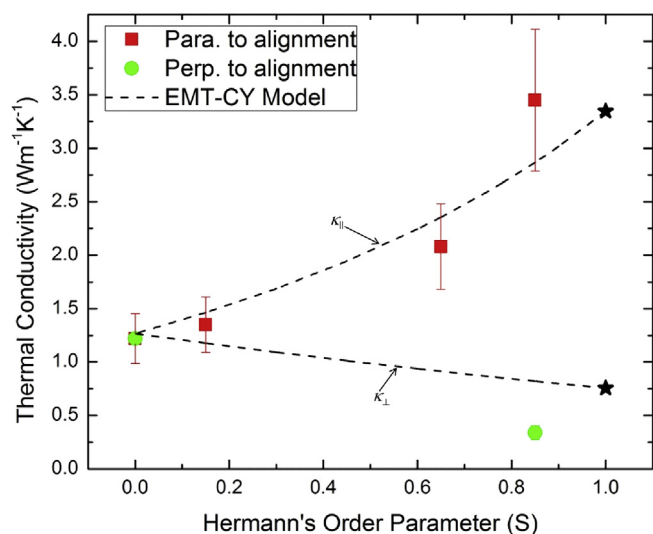


Fig. 7. Experimental κ of anisotropic CNC-PVA composite films shown along with results from the EMT-CY model as a function of S . The weight % of CNC is not in particular order. The stars represent the extrapolated values of κ obtained from the EMT-CY model at $S \approx 1$.

direction. The orientation angle of the crystals with respect to the shear direction is represented by γ , while $\kappa_{c\parallel}$ and $\kappa_{c\perp}$ represent the thermal conductivities of a single CNC in the axial and the transverse crystalline directions respectively and their corresponding values were predicted to be $\sim 5.7 \text{ W m}^{-1} \text{ K}^{-1}$ and $\sim 0.72 \text{ W m}^{-1} \text{ K}^{-1}$ by Diaz et al. [30].

Fig. 7 shows the experimentally obtained values of the κ of anisotropic CNC-PVA composite films along with those predicted by the EMT-CY model in the directions parallel (κ_{\parallel}) and perpendicular (κ_{\perp}) to the shear direction. This model predicts a κ of $\sim 1.27 \text{ W m}^{-1} \text{ K}^{-1}$ for an isotropic film which is close to that of the experimental value ($\sim 1.22 \text{ W m}^{-1} \text{ K}^{-1}$). The model also predicts the upper bound and lower bound values of κ_m to be $\sim 1.23 \text{ W m}^{-1} \text{ K}^{-1}$ and $\sim 0.46 \text{ W m}^{-1} \text{ K}^{-1}$, respectively. The lower end of this range is comparable to the upper end of the experimentally obtained κ value of neat PVA, specifically $\sim 0.08 \text{ W m}^{-1} \text{ K}^{-1}$ to $\sim 0.41 \text{ W m}^{-1} \text{ K}^{-1}$ for initial PVA weight % of 1%–10.7%. This close agreement between κ_m and the κ of neat PVA suggests that other contributions to interfacial thermal resistance such as CNC–CNC or CNC–matrix interfaces are relatively small in comparison. In addition, the values of κ_m obtained are significantly larger than the effective κ_m value of $0.022 \text{ m}^{-1} \text{ K}^{-1}$ obtained in our previous work on CNC-only films [30]. Together, these insights show that the addition of PVA as an interstitial secondary material can have significant positive influence on the effective κ of CNC-based films, likely due to the removal of free volume and nanoscopic voids, which have extremely high effective resistance.

Relative to competitor materials, Table 1 shows that the in-plane κ of the best performing CNC-PVA composite film developed in this work is ~ 4 –14 times higher than that of other plastic films that are currently used for transparent, flexible devices indicating the potential of the CNC-PVA composite films an application for thermal management of flexible electronic devices. Regarding other CN-based materials the results presented here are ~ 1.4 times higher than that of the TNW sheet developed by Uetani et al. [22] However, there are significant differences between the work here and Uetani. Primarily, the best results of Uetani were for Tunicate Nanowhiskers (TNWs) which are significantly longer (microns) than the wood-based CNCs here (100 nm) [23]. As Diaz et al. showed that the long axis has a much higher κ than either orthogonal direction, the isotropic TNW materials should show much higher κ than the isotropic wood-based CNCs here, which is the case. However, the TNW materials show high effective interfacial resistance and low sound velocity in direct contrast to Diaz, although as

Uetani stated, this was at least partially due to small pores in the structure. Thus, reduction of interfacial resistance, and a concomitant increase in κ , would be expected to result from filling the free volume/small pores with a strongly bonded solid material. Additionally, Uetani showed a strong correlation with nanocrystal width, with TNW showing the highest κ , ostensibly as it was the widest material. Notwithstanding the correlation of width to length of the materials, which would have a large effect as described above, an isotropic random arrangement of CNC or TNW, as in a random mat, would be expected to have a large percentage of crossed crystal contact points. As contact points are where nearly all heat transport takes place and cross-points have less contact area than parallel axial contact along the width, it would be expected that isotropic arrangements would have higher effective interfacial resistance than anisotropic axial arrangements due to the higher amount cross-points relative to parallel axial contacts leading to less overall contact area to transport heat in the isotropic arrangement. Interestingly, as seen in Uetani, logically one would assume a high dependence on crystal width as, in a given volume, there would be more intracrystalline transport as opposed to across interfaces for larger widths. Regardless, combining the data sets, while the work here has a high κ , we should expect even higher for aligned composite structures of longer materials such as TNW.

The CNC-PVA composite films developed through this work show the potential for dissipating a significant amount of heat from electronics-like concentrated heat sources. Fig. 8 shows thermal images obtained from a 100% PVA sample and a CNC-PVA (90:10) sample as a demonstration of their relative ability to dissipate heat away from a localized hot spot. Identical serpentine gold heaters were shadow-evaporated on the surface of each of these samples and the same Joule heating power (175 mW) induced via a DC power supply. Thermal images were taken using almost identical temperature scales. As can be observed, the maximum temperature of the resulting hot spot for the CNC: PVA composite sample was significantly lower ($\sim 7^\circ \text{C}$) than that of the neat PVA sample. The DC power was applied across the top left and bottom right contact pads of both samples, which results in the slight asymmetry as seen in the images.

4. Conclusion

In this work, CNC-PVA composite films consisting of PVA of different molecular weights and different CNC: PVA ratios were prepared with a variation of S between 0 and 0.85 for anisotropic films. The measurement of the κ showed significant improvement on isotropic CNC-PVA films with 10–50 wt% PVA solid loading compared to one component system. Further, the anisotropic composite films showed κ as high as $\sim 3.45 \text{ W m}^{-1} \text{ K}^{-1}$ in the shear direction which was a $\sim 2.5\text{X}$ improvement over the CNC-PVA composite films with the isotropic configuration. Such improvements on κ of CNC-PVA composite films can be attributed to the role of PVA as excellent void filling agent for forming conductive paths for phonon transport with reduced interfacial resistance and the orientation of CNCs towards heat flow direction in anisotropic films. Compared to the commonly used plastic films for flexible electronic devices, our CNC-PVA composite films showed ~ 4 –14 fold higher κ while also demonstrating better heat spreading capability from a localized hot spot as would be experienced by a flexible electronics element. These results provide the basis for use of CNC-PVA composite films as substrates for potential application in the thermal management of flexible electronics and can be an eco-friendly and sustainable alternative to the petroleum-based polymeric materials.

Author contributions

The manuscript was written through contributions of all authors. All authors have given approval to the final version of the manuscript. ^a These authors contributed equally.

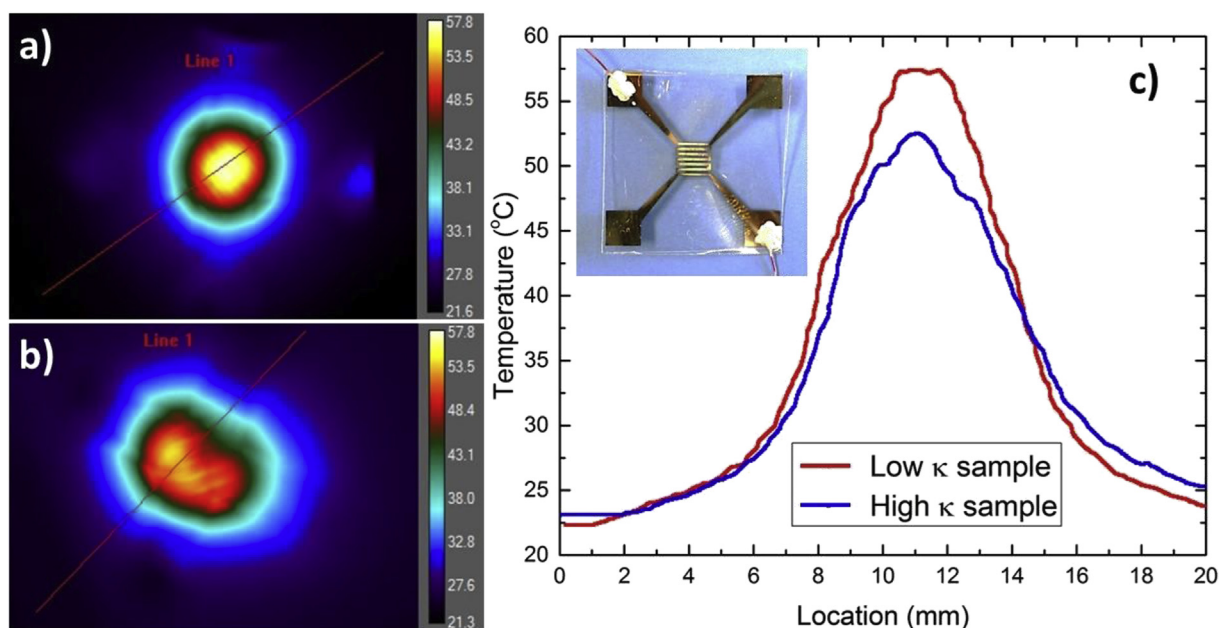


Fig. 8. Thermal images of CNC-PVA composites a) 100% PVA sample with low κ , and b) 90:10 CNC:PVA sample with high κ during Joule heating of a serpentine metallic heater simulating flexible electronics elements. c) Line scans along the centerline of a) and b) quantify the temperature reduction associated with the high κ sample at the same Joule heating power (175 mW). Inset: Photograph of 90:10 CNC:PVA sample with shadow-evaporated metallic heater.

Acknowledgements

The research was partially supported by the National Science Foundation Scalable Nanomanufacturing program under award CMMI-1449358. This work was partially supported through a grant from the National Science Foundation Materials Engineering and Processing program under award CMMI-1636289. Additional support provided by start-up funding from Louisiana Tech University.

Appendix A. Supplementary data

Supplementary data to this article can be found online at <https://doi.org/10.1016/j.polymer.2019.01.006>.

References

- [1] H. Chen, V.V. Ginzburg, J. Yang, Y. Yang, W. Liu, Y. Huang, L. Du, B. Chen, Thermal conductivity of polymer-based composites: fundamentals and applications, *Prog. Polym. Sci.* 59 (2016) 41–85.
- [2] A.R.J. Hussain, A.A. Alahyari, S.A. Eastman, C. Thibaud-Erkey, S. Johnston, M.J. Sobkowicz, Review of polymers for heat exchanger applications: factors concerning thermal conductivity, *Appl. Therm. Eng.* 113 (2017) 1118–1127.
- [3] Q. Xue, J. Sun, Electrical conductivity and percolation behavior of polymer nanocomposites, *Polymer Nanocomposites* (2016) 281–322 Springer.
- [4] X. Liu, Y.-Z. Long, L. Liao, X. Duan, Z. Fan, Large-scale integration of semiconductor nanowires for high-performance flexible electronics, *ACS Nano* 6 (3) (2012) 1888–1900.
- [5] H. Zhu, Z. Xiao, D. Liu, Y. Li, N.J. Weadock, Z. Fang, J. Huang, L. Hu, Biodegradable transparent substrates for flexible organic-light-emitting diodes, *Energy Environ. Sci.* 6 (7) (2013) 2105–2111.
- [6] Y. Zhou, C. Fuentes-Hernandez, T.M. Khan, J.-C. Liu, J. Hsu, J.W. Shim, A. Dindar, J.P. Youngblood, R.J. Moon, B. Kippelen, Recyclable organic solar cells on cellulose nanocrystal substrates, *Sci. Rep.* 3 (2013) 1536.
- [7] D. Rule, D. Smith, L.L. Sparks, Thermal Conductivity of a Polyimide Film between 4.2 and 300K, with and without Alumina Particles as Filler, (1990).
- [8] N. Balachander, I. Seshadri, R.J. Mehta, L.S. Schadler, T. Borca-Tasciuc, P. Keblinski, G. Ramanath, Nanowire-filled polymer composites with ultrahigh thermal conductivity, *Appl. Phys. Lett.* 102 (9) (2013) 093117.
- [9] P. Yi, R.A. Awang, W.S. Rowe, K. Kalantar-Zadeh, K. Khoshmanesh, PDMS nanocomposites for heat transfer enhancement in microfluidic platforms, *Lab Chip* 14 (17) (2014) 3419–3426.
- [10] P. Lee, J. Lee, H. Lee, J. Yeo, S. Hong, K.H. Nam, D. Lee, S.S. Lee, S.H. Ko, Highly stretchable and highly conductive metal electrode by very long metal nanowire percolation network, *Adv. Mater.* 24 (25) (2012) 3326–3332.
- [11] D. Slee, J. Stepan, W. Wei, J. Swart, Introduction to printed circuit board failures, *Product Compliance Engineering*, 2009, PSES 2009. IEEE Symposium on, IEEE, 2009, pp. 1–8.
- [12] M.Z.M. Hanafi, F.S. Ismail, R. Rosli, Radial plate fins heat sink model design and optimization, *Control Conference (ASCC)*, 2015 10th Asian, IEEE, 2015, pp. 1–5.
- [13] S. Bhanushali, N.N. Jason, P. Ghosh, A. Ganesh, G.P. Simon, W. Cheng, Enhanced thermal conductivity of copper nanofluids: the effect of filler geometry, *ACS Appl. Mater. Interfaces* 9 (22) (2017) 18925–18935.
- [14] Y. Zhang, Y.-J. Heo, Y.-R. Son, I. In, K.-H. An, B.-J. Kim, S.-J. Park, Recent advanced thermal interfacial materials: A review of conducting mechanisms and parameters of carbon materials, *Carbon* 142 (2018) 445–460.
- [15] Y. Zhang, J.R. Choi, S.-J. Park, Enhancing the heat and load transfer efficiency by optimizing the interface of hexagonal boron nitride/elastomer nanocomposites for thermal management applications, *Polymer* 143 (2018) 1–9.
- [16] K. Pratik, A. Rai, T.S. Ashton, A.L. Moore, APCVD hexagonal boron nitride thin films for passive near-junction thermal management of electronics, *Nanotechnology* 28 (50) (2017) 505705.
- [17] A. Rai, A.L. Moore, Enhanced thermal conduction and influence of interfacial resistance within flexible high aspect ratio copper nanowire/polymer composites, *Compos. Sci. Technol.* 144 (2017) 70–78.
- [18] F.E. Alam, W. Dai, M. Yang, S. Du, X. Li, J. Yu, N. Jiang, C.-T. Lin, In situ formation of a cellular graphene framework in thermoplastic composites leading to superior thermal conductivity, *J. Mater. Chem.* 5 (13) (2017) 6164–6169.
- [19] H. Wu, L.T. Drzal, Graphene nanoplatelet paper as a light-weight composite with excellent electrical and thermal conductivity and good gas barrier properties, *Carbon* 50 (3) (2012) 1135–1145.
- [20] S.M. Hamidinejad, R.K. Chu, B. Zhao, C.B. Park, T. Filleter, Enhanced thermal conductivity of graphene nanoplatelet-polymer nanocomposites fabricated via supercritical fluid assisted in-situ exfoliation, *ACS Appl. Mater. Interfaces* 10 (1) (2017) 1225–1236.
- [21] J. Gonzalez-Gutierrez, I. Duretek, C. Kukla, A. Poljšak, M. Bek, I. Emri, C. Holzer, Models to predict the viscosity of metal injection cellulose nanofiber materials as function of their formulation, *Metals* 6 (6) (2016) 129.
- [22] K. Uetani, T. Okada, H.T. Oyama, Crystallite size effect on thermal conductive properties of nonwoven nanocellulose sheets, *Biomacromolecules* 16 (7) (2015) 2220–2227.
- [23] R.J. Moon, A. Martini, J. Nairn, J. Simonsen, J. Youngblood, Cellulose nanomaterials review: structure, properties and nanocomposites, *Chem. Soc. Rev.* 40 (7) (2011) 3941–3994.
- [24] Y. Shimazaki, Y. Miyazaki, Y. Takezawa, M. Nogi, K. Abe, S. Ifuku, H. Yano, Excellent thermal conductivity of transparent cellulose nanofiber/epoxy resin nanocomposites, *Biomacromolecules* 8 (9) (2007) 2976–2978.
- [25] K. Uetani, T. Okada, H.T. Oyama, Thermally conductive and optically transparent flexible films with surface-exposed nanocellulose skeletons, *J. Mater. Chem. C* 4 (41) (2016) 9697–9703.
- [26] A.B. Reising, R.J. Moon, J.P. Youngblood, Effect of Particle Alignment on Mechanical Properties of Neat Cellulose Nanocrystal Films, (2012).
- [27] J.A. Diaz, X. Wu, A. Martini, J.P. Youngblood, R.J. Moon, Thermal expansion of self-organized and shear-oriented cellulose nanocrystal films, *Biomacromolecules* 14 (8) (2013) 2900–2908.
- [28] R.A. Chowdhury, S.X. Peng, J. Youngblood, Improved order parameter (alignment) determination in cellulose nanocrystal (CNC) films by a simple optical birefringence method, *Cellulose* 24 (5) (2017) 1957–1970.

- [29] E.E. Ureña-Benavides, G. Ao, V.A. Davis, C.L. Kitchens, Rheology and phase behavior of lyotropic cellulose nanocrystal suspensions, *Macromolecules* 44 (22) (2011) 8990–8998.
- [30] J.A. Diaz, Z. Ye, X. Wu, A.L. Moore, R.J. Moon, A. Martini, D.J. Boday, J.P. Youngblood, Thermal conductivity in nanostructured films: from single cellulose nanocrystals to bulk films, *Biomacromolecules* 15 (11) (2014) 4096–4101.
- [31] R.A. Chowdhury, C. Clarkson, J. Youngblood, Continuous roll-to-roll fabrication of transparent cellulose nanocrystal (CNC) coatings with controlled anisotropy, *Cellulose* 25 (3) (2018) 1769–1781.
- [32] D. Benford, T. Powers, S. Moseley, Thermal conductivity of Kapton tape, *Cryogenics* 39 (1) (1999) 93–95.
- [33] J.P. Lagerwall, C. Schütz, M. Salajkova, J. Noh, J.H. Park, G. Scalia, L. Bergström, Cellulose nanocrystal-based materials: from liquid crystal self-assembly and glass formation to multifunctional thin films, *NPG Asia Mater.* 6 (1) (2014) e80.
- [34] X.M. Dong, T. Kimura, J.-F. Revol, D.G. Gray, Effects of ionic strength on the isotropic – chiral nematic phase transition of suspensions of cellulose crystallites, *Langmuir* 12 (8) (1996) 2076–2082.
- [35] G.-H. Kim, D. Lee, A. Shanker, L. Shao, M.S. Kwon, D. Gidley, J. Kim, K.P. Pipe, High thermal conductivity in amorphous polymer blends by engineered interchain interactions, *Nat. Mater.* 14 (3) (2015) 295.
- [36] N. Burger, A. Laachachi, M. Ferriol, M. Lutz, V. Toniazzo, D. Ruch, Review of thermal conductivity in composites: mechanisms, parameters and theory, *Prog. Polym. Sci.* 61 (2016) 1–28.
- [37] D.G. Cahill, W.K. Ford, K.E. Goodson, G.D. Mahan, A. Majumdar, H.J. Maris, R. Merlin, S.R. Phillpot, Nanoscale thermal transport, *J. Appl. Phys.* 93 (2) (2003) 793–818.
- [38] C.-W. Nan, R. Birringer, Determining the Kapitza resistance and the thermal conductivity of polycrystals: a simple model, *Phys. Rev. B* 57 (14) (1998) 8264.
- [39] S.T. Huxtable, D.G. Cahill, S. Shenogin, L. Xue, R. Ozisik, P. Barone, M. Usrey, M.S. Strano, G. Siddons, M. Shim, Interfacial heat flow in carbon nanotube suspensions, *Nat. Mater.* 2 (11) (2003) 731.
- [40] C. Choy, Thermal conductivity of polymers, *Polymer* 18 (10) (1977) 984–1004.
- [41] G. Cieloszyk, M. Cruz, G. Salinger, Thermal properties of dielectric solids below 4 K I—polycarbonate, *Cryogenics* 13 (12) (1973) 718–721.
- [42] C. Choy, W. Luk, F. Chen, Thermal conductivity of highly oriented polyethylene, *Polymer* 19 (2) (1978) 155–162.
- [43] C. Choy, K. Young, Thermal conductivity of semicrystalline polymers—a model, *Polymer* 18 (8) (1977) 769–776.
- [44] C. Choy, F. Chen, W. Luk, Thermal conductivity of oriented crystalline polymers, *J. Polym. Sci. B Polym. Phys.* 18 (6) (1980) 1187–1207.